Longitudinal phonon plasmon mode coupling in β -Ga₂O₃

Mathias Schubert, 1,2,3,a) Alyssa Mock, Rafał Korlacki, Sean Knight, Zbigniew Galazka, Günther Wagner, Gunther Wagner, Virginia Wheeler, Marko Tadjer, Ken Goto, and Vanya Darakchieva³

¹⁾Department of Electrical and Computer Engineering, University of Nebraska-Lincoln, Lincoln, NE 68588,

(Dated: 19 February 2019)

In this letter, we investigate a set of *n*-type single crystals of monoclinic symmetry β -Ga₂O₃ with different free electron concentration values by generalized far infrared and infrared spectroscopic ellipsometry. In excellent agreement with our previous model prediction, we find here by experiment that longitudinal-phonon-plasmon coupled modes are polarized either within the monoclinic plane or perpendicular to the monoclinic plane. As predicted, all modes change amplitude and frequency with the free electron concentration. The most important observation is that all longitudinalphonon-plasmon coupled modes polarized within the monoclinic plane continuously change their direction as a function of free electron concentration.

The single crystalline form of gallium (III) oxide with monoclinic crystal structure, β-Ga₂O₃, has gained substantial interest most recently for its potential use in high voltage electronic applications. 1,2 Its direct band gap is very large, reported in a range from 4.8 eV to 5.04 eV.3-8 A breakdown electric field of more than double of the theoretical limits for SiC and GaN is predicted, which would result in more than triple their power device performance.² Applications as transparent electrodes,⁹ smart windows,^{10,11} photovoltaic cells,¹⁰ and gas sensors have been reported. 12 It was shown recently that β-Ga₂O₃ has the highest lifetime optical damage performance of any conductive material measured to date, above 10 J/cm² (1.4 GW/cm²).¹³ Very importantly, single crystalline high-quality β-Ga₂O₃ can be grown with a wide range of *n*-type conductivity, from $\approx 1 \times 10^{15} \text{ cm}^{-3} \text{ to } \approx 1 \times 10^{20}$ cm⁻³ by unintentional or intentional donor doping in bulk and epitaxial materials.2 Correct and accurate characterization of free charge carrier properties in bulk and heteroepitaxial layer structures is a crucial step in successful design of semiconductor heterostructure devices. Long-wavelength (infrared and farinfrared) optical spectroscopy, in particular ellipsometry, is a traditional tool to investigate the effect of free charge carriers onto the optical response of semiconductor materials, even if part of complex layer structures.¹⁴ At long wavelengths, specifically in materials with polar lattice resonances, collective free charge carrier excitations, plasmons, couple with the lattice vibration modes. 15-17 This effect and related phenomena observable in optical spectroscopies are well known for materials with crystal symmetries higher than or equal to orthorhombic, for example, in zincblende-structure (cubic) GaAs, ¹⁸ InSb, ¹⁹ InAs¹⁹, or wurtzite-structure (hexagonal) CdS, ²⁰ ZnO, ²¹ GaN, ^{22,23} InN, ²⁴ or rutile-structure (tetragonal) SnO₂.²⁵ In all such cases, coupling of longitudinal optical (LO) phonons with collective plasma oscillations (plasmons) occurs along high-symmetry directions of the lattice. The coupled modes, while changing their frequencies with increasing free charge carrier density maintain the polarization direction of the LO phonons at zero free charge carrier density. In semiconductors with monoclinic symmetry, such as β -Ga₂O₃, plasmons also couple with LO phonons. In our recent work, we have shown that LO phonons within the monoclinic plane of β -Ga₂O₃ are not polarized parallel to any of the lowindex crystallopgrahic directions.²⁶ Instead, their directions, at first sight, appear to be randomly distributed. However, upon closer inspection, it becomes clear that the LO mode directions are tied to the specific values of all amplitude, direction, and frequency parameters of all transverse optical (TO) lattice modes.²⁷ We have further identified that LO modes are affected by free charge carriers, and form longitudinalphonon-plasmon (LPP) coupled modes. In Ref. 26 we hypothesized about the behavior of the LPP modes as a function of the free charge carrier density, and we predicted that all eigendielectric displacement directions of the LPP modes would vary with free charge carrier density. We also hypothesized that the order of the LPP modes with respect to the TO modes would change. However, in our previous work,²⁶ only specimens with approximately the same free electron density were investigated, and the variation of LPP modes with free electron density remained experimentally unexplored. Verification of LPP mode properties is important, for example, to reliably calculate effects of electron-phonon interaction and high electric fields onto electronic transport properties. ^{28–31} In this letter, we present the result of an investigation of LPP modes in a set of samples with free electron density parameter varying from $\approx 5 \times 10^{17} \text{ cm}^{-3}$ to $\approx 6 \times 10^{18} \text{ cm}^{-3}$.

The derivations of the LPP mode parameters and the

phonon mode order in monoclinic crystals follow closely the

²⁾Leibniz Institute for Polymer Research, Dresden, 01069, Germany

³⁾Terahertz Materials Analysis Center, Department of Physics, Chemistry and Biology, Linköping University, SE 58183, Linköping,

⁴⁾Leibniz-Institut für Kristallzüchtung, Berlin, 12489, Germany

⁵⁾United States Naval Research Laboratory, Washington, DC 20375, U.S.A.

⁶⁾Novel Crystal Technology, Inc., Saitama-ken 350-1328, Japan

original reports in Ref. 26 and Ref. 27, respectively, which due to space limitations are kept minimal here. The long wavelength dependencies of the dielectric function tensor, $\varepsilon(\omega)$, and the dielectric loss function tensor, $\varepsilon^{-1}(\omega)$, can be de-

a) Electronic mail: schubert@engr.unl.edu; http://ellipsometry.unl.edu

scribed by two sets of eigenmodes – the TO and LO phonon modes, and wavelength independent polarizability contributions (ε_{∞}) due to electronic and excitonic excitations at photon energies much higher than all lattice mode frequencies. ^{16,17,32} TO modes occur at frequencies at which dielectric resonance occurs for electric fields along $\hat{\mathbf{e}}_l$ with eigendielectric displacement unit vectors then defined as $\hat{\mathbf{e}}_l = \hat{\mathbf{e}}_{\text{TO},l}$. ³³ Similarly, LO modes occur when the dielectric loss approaches infinity for electric fields along $\hat{\mathbf{e}}_l$ with eigendielectric displacement unit vectors then defined as $\hat{\mathbf{e}}_l = \hat{\mathbf{e}}_{\text{LO},l}$. ¹⁶ An eigendielectric displacement vector summation (EDVS) approach was introduced recently, ^{26,27,34,35} where ε is composed of sums of dyadics, ($\hat{\mathbf{e}}_{\text{TO},l} \otimes \hat{\mathbf{e}}_{\text{TO},l}$), scaled with frequency-dependent complex-valued response functions, $\varrho_{\text{TO},l}$

$$\varepsilon = \varepsilon_{\infty} + \sum_{l=1}^{N} \varrho_{\text{TO},l}(\hat{\mathbf{e}}_{\text{TO},l} \otimes \hat{\mathbf{e}}_{\text{TO},l}), \tag{1}$$

where the index l denotes all TO modes within the monoclinic lattice. In the absence of doping, β -Ga₂O₃ possesses 8 B_u -symmetry TO modes polarized within the monoclinic lattice plane, and 4 A_u -symmetry TO modes polarized parallel to the lattice axis b. The inverse of ε is obtained by an eigendielectric displacement loss vector summation (EDLVS) approach³⁶

$$\varepsilon^{-1} = \varepsilon_{\infty}^{-1} - \sum_{l=1}^{N} \varrho_{\mathrm{LO},l}(\hat{\mathbf{e}}_{\mathrm{LO},l} \otimes \hat{\mathbf{e}}_{\mathrm{LO},l}), \tag{2}$$

where the index l denotes all LO modes within the monoclinic lattice. Anharmonically broadened Lorentzian oscillator functions can be used to describe functions ρ in Eqs. 1 and 2.

$$\varrho_{k,l}(\omega) = \frac{A_{k,l}^2 - i\Gamma_{k,l}\omega}{\omega_{k,l}^2 - \omega^2 - i\omega\gamma_{k,l}}.$$
 (3)

Here, $A_{k,l}$, $\omega_{k,l}$, $\gamma_{k,l}$, and $\Gamma_{k,l}$ denote amplitude, resonance frequency, harmonic broadening, and anharmonic broadening parameters for TO (k="TO") or LO (k="LO") mode l, respectively, and ω is the frequency of the driving electromagnetic field. We note a misprint in Eq. 10 of Ref. 26 where the square on the amplitude parameter was erroneously omitted.

The contributions of free charge carriers to ε are augmented using the Drude model for free charge carriers.¹⁴ In order to account for the three dimensional nature of the motion of free charge carriers, and their directional anisotropy for transport properties (optical mobility parameters), free charge carrier contributions are augmented by 3 additional terms to Eq. 1

$$\varepsilon_{\text{LPP}} = \varepsilon + \sum_{l=1}^{3} \varrho_{\text{TO}=0,l}(\hat{\mathbf{e}}_{\text{TO}=0,l} \otimes \hat{\mathbf{e}}_{\text{TO}=0,l}). \tag{4}$$

We select directions $\hat{\mathbf{e}}_{TO=0,l}$ to coincide with Cartesian coordinate axes (x, y, z). The definition of the Cartesian axes with respect to the crystal unit cell of β -Ga₂O₃ is described in the Supplementary Material. Briefly, crystal axes a and c are within the monoclinic plane, and axis b is perpendicular to the monoclinic plane. \mathbf{a} is parallel to x, \mathbf{b} is antiparallel to

z, and \mathbf{c} is within the (x, y) plane. $\varrho_{\text{TO}=0, l}$ can be expressed as follows

$$\varrho_{\text{TO}=0,(x,y,z)} = -\frac{e^2 N}{\tilde{\varepsilon}_0 m^{\star}_{(x,y,z)} m_e \omega(\omega + i \gamma_{\text{p},(x,y,z)})}, \tag{5}$$

where N is the free charge carrier volume density parameter, e is the electronic charge, m_e is the free electron mass, $m_{(x,y,z)}^{\star}$ are the three directional effective mass parameters, and the directional plasma broadening parameters $\gamma_{p,(x,y,z)}$ are connected with the directional optical mobility parameters

$$\mu_{(x,y,z)} = \frac{e}{\tilde{\varepsilon}_0 m_{(x,y,z)}^{\star} m_{\rm e} \gamma_{\rm p,(x,y,z)}}.$$
 (6)

The plasma frequency parameter is then also dependent on polarization direction

$$\omega_{p,(x,y,z)}^2 = \frac{e^2 N}{m_{(x,y,z)}^* m_e},\tag{7}$$

and can be considered as an isotropic value when the effective mass parameters are isotropic. For β -Ga₂O₃ it was found in recent optical Hall effect measurements that the bottom conduction band effective mass parameter is isotropic, and $m_x^* = m_y^* = m_z^* = 0.28.^{37}$

Analogously, three terms are added for ε^{-1} .

$$\varepsilon_{\text{LPP}}^{-1} = \varepsilon^{-1} - \sum_{l=1}^{N+3} \varrho_{\text{LPP},l}(\hat{\mathbf{e}}_{\text{LPP},l} \otimes \hat{\mathbf{e}}_{\text{LPP},l}). \tag{8}$$

We note that while the addition of 3 Drude terms to Eq. 1 does not change the TO mode parameters, all LO mode parameters change in Eq. 2 upon the addition of the three terms in Eq. 8 reflecting the LPP mode coupling. For polarization within the monoclinic plane, i.e., modes with $B_{\rm u}$ -symmetry, and for a single species free charge carrier density (such as single band holes, or single band electrons) two TO modes with zero frequency $\omega_{TO} = 0$ must be added to Eq. 4, hence, 10 TO modes exist, and 10 associated LPP modes must occur in Eq. 8, oriented (polarized) within the monoclinic a-c plane. For polarization perpendicular to the monoclinic plane, i.e., modes with $A_{\rm u}$ -symmetry, one TO mode with zero frequency $\omega_{\rm TO}$ is added to Eq. 4, hence, the displacement directions of 5 TO modes and 5 associated LPP modes (A_u symmetry) are oriented perpendicular to the monoclinic plane. Thus all eigenvectors are aligned with axis b. Hence, for $B_{\rm u}$ - and $A_{\rm u}$ -symmetry LPP modes, $\hat{\mathbf{e}}_{LPP,l} = \cos \alpha_{LPP,l} \hat{\mathbf{x}} + \sin \alpha_{LPP,l} \hat{\mathbf{y}}$, and $\hat{\mathbf{e}}_{LPP,l} = -\hat{\mathbf{z}}$, respectively. Thereby, we have introduced the parameters $\alpha_{LPP,l}$ representing the directions of the LPP modes. The directions can be determined as a function of the electron density, or equivalently, $\omega_{\rm p}$. After setting all broadening parameters in Eqs. 3 and 5 to zero, the LPP mode parameters $\omega_{LPP,l}$, $\alpha_{LPP,l}$, and $A_{LPP,l}$ follow from the following relations, respectively (See also Supplementary Materials): ^{26,34}

$$\det\{\varepsilon_{\text{LPP}}(\omega = \omega_{\text{LPP},l})\} \to 0, \tag{9}$$

$$\varepsilon(\omega = \omega_{\text{LPP},l})\hat{\mathbf{e}}_{\text{LPP},l} = 0, \tag{10}$$

$$(\varepsilon_{\rm LPP})^{-1} = \varepsilon_{\rm LPP}^{-1}. \tag{11}$$

We have performed series of long-wavelength ellipsometry measurements on a set of different bulk single crystals with various surface orientations, and different free electron density parameters. Details of the experimental procedures and sample descriptions are given in Ref. 26 and the Supplementary Material, respectively. Selected experimental and best-model calculated ellipsometry data are shown in the Supplementary Material and omitted here for brevity. We have analyzed all ellipsometry data by using the model dielectric function tensor approach discussed in Ref. 26. We have analyzed data from every sample separately. As a result, we determined the best-match model calculated plasma frequency parameter and the mobility parameters for all three major axes directions, a, \mathbf{c}^{\star} , and **b**. Results for the mobility parameters are not further discussed here. The LPP mode parameters are calculated from the best-match model calculated dielectric function tensor after setting all phonon mode and plasma broadening parameters to zero. The results of the LPP mode parameters are included into Figs. 1, 2, and 3, which are discussed below.

Figures 1a-c depict the dependencies of the LPP mode parameters as a function of ω_p . The solid lines in Figs. 1a-c are calculated with phonon mode parameters determined in Ref. 26. The symbols in Figs. 1a-c indicate the parameters obtained from set of samples investigated by ellipsometry in this work. An excellent match between the hypothesized behavior (solid lines) and the experimental observation (symbols) is noted. At small ω_p , 2 additional LPP branches emerge from zero (labeled 9 and 10 in Figs. 1a-c), polarized within the monoclinic plane. With increasing $\omega_{\rm p}$, the LPP frequencies (Fig. 1a) shift away from their originating LO modes at $\omega_p = 0$. The phonon mode order changes gradually, whereby frequencies of $B_{\rm u}$ -LPP modes 5, 6, and 9 cross frequencies of TO modes IV, V, and VIII (Fig. 1a), respectively. Such an occurrence is never observed for semiconductors with symmetry higher than monoclinic. The two highest $B_{\rm u}$ -LPP branches approach infinity for $\omega_p \to \infty$. The amplitude parameters reflect the coupling behavior between LO and plasmon modes. The two additional modes, labeled 9 and 10, represent the plasmon-like behavior for small ω_p . Note also the linear increase for their frequencies. For intermediate carrier densities, all amplitudes begin to diminish, except for the 2 modes with largest frequencies, labeled 1 and 2. These are the plasmonlike modes for very large ω_p . Accordingly, while all amplitudes of all other modes approach zero eventually, the amplitudes of modes labeled 1 and 2 approach infinity for $\omega_p \to \infty$. Figure 1c depicts the evolution of the LPP angular orientation, which represents the displacement direction of the associated lattice motion.³⁸ Contrary to the behavior of LPP modes in semiconductors with symmetry higher than monoclinic, the LPP mode lattice displacement directions continuously shift with increasing ω_p . For very large ω_p , all directions approach eventually one of the TO mode displacement directions. This variation is not random, and will be addressed further below.

Figures 2a-b depicts the same as Fig. 1a-c for the $A_{\rm u}$ -LPP modes. An excellent match between the hypothesized behavior (solid lines) and the experimental observation (symbols) is noted. The behavior observed here is very similar to LPP

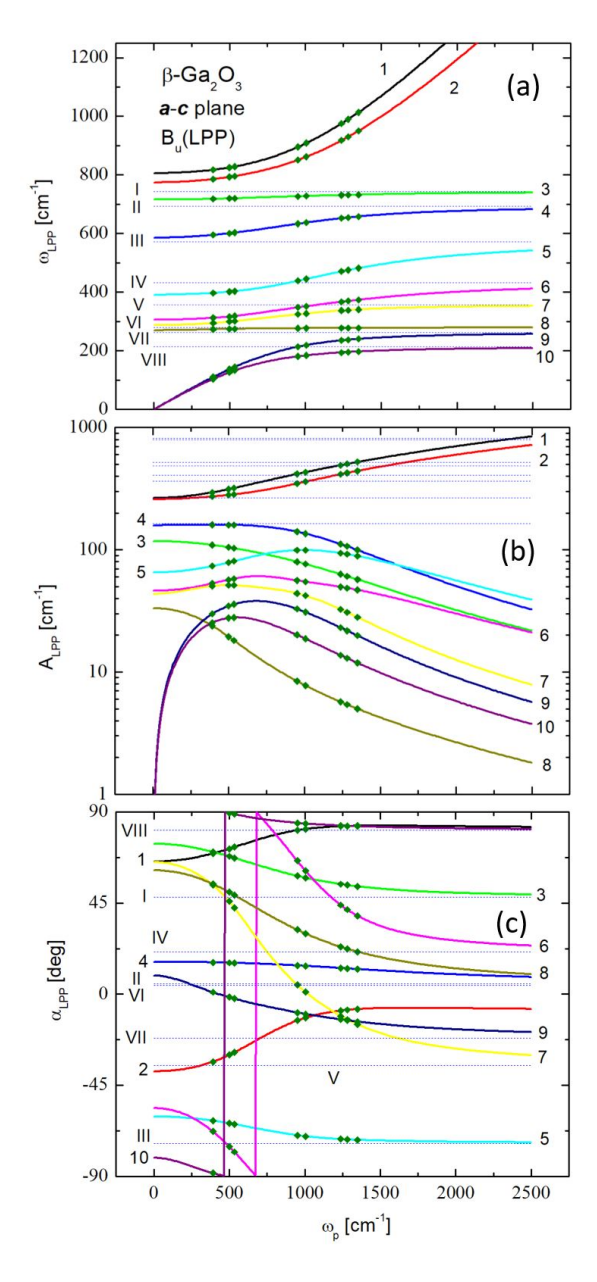


FIG. 1. $B_{\rm u}$ -symmetry LPP mode parameters as a function of $\omega_{\rm p}$, (a) frequency, (b) amplitude, (c) angular direction relative to axis a within the ${\bf a}-{\bf c}$ plane. Horizontal lines and roman numerals indicate corresponding parameters of the TO modes. Symbols (diamonds) indicate the results from experiment obtained in this work. Numerical data are given in the Supplementary Materials.

mode coupling in semiconductors with multiple phonon mode branches and symmetries higher than monoclinic. At small ω_p , one additional branch emerges from zero. With increasing ω_p , the LPP modes shift away from their associated LO mode frequencies at $\omega_p=0$, but do not change the phonon mode order. The highest frequency mode approaches infinity for $\omega_p\to\infty$. Likewise, the amplitude of the highest LPP mode

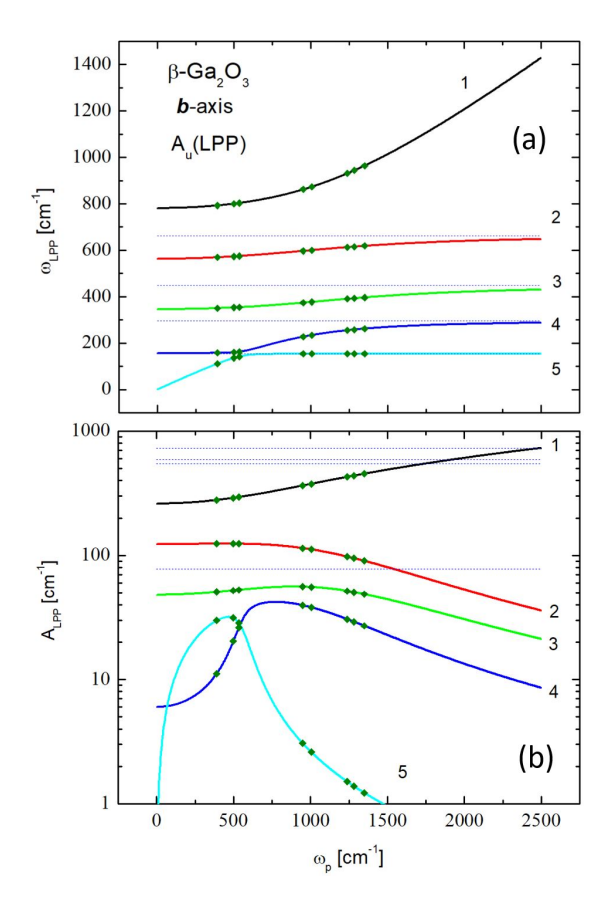


FIG. 2. $A_{\rm u}$ -symmetry LPP mode parameters as a function of $\omega_{\rm p}$, (a) frequency, and (b) amplitude. Note that all angular parameters are parallel to axis b. Horizontal lines indicate corresponding parameters of the TO modes. Symbols (diamonds) indicate the results from experiment obtained in this work. Numerical data are given in the Supplementary Materials.

approaches infinity for very large plasma frequency while all other amplitudes approach zero.

Within the Born and Huang approach,³³ which permits calculation of the lattice dynamic properties in crystals with arbitrary symmetry, solutions with $\mathbf{E} \neq 0$ and $\mathbf{D} \neq 0$ define the so-called limiting frequencies $\omega(\alpha)_l$.³⁹ Here, α parameterizes the lattice displacement direction of $\omega(\alpha)_l$ within the monoclinic plane. We recently showed that $\omega(\alpha)_l$ can be determined from analysis of experimental ellipsometry data, and we provided an explanation for the order of all TO, LO, and $\omega(\alpha)_l$ modes in crystals with monoclinic symmetry without free charge carriers.²⁷ In the case of LPP mode coupling, modes $\omega(\alpha)_l$ also couple, and may be termed $\omega(\alpha)_{\text{LPP},l}$. Figure 3 depicts $\omega(\alpha)_{\text{LPP},l}$ for different values of ω_p . For $\omega_p = 0$, Fig. 3 is identical with Fig. 1c in Ref. 27, and which is explained there in detail. Here, we demonstrate the effect of plasmon coupling.

Modes $\omega(\alpha)_{\text{LPP},l}$ in Fig. 3 are bound between TO and LPP modes. LPP modes shift with ω_{p} , and $\omega(\alpha)_{\text{LPP},l}$ change accordingly. There are 10 modes of $\omega(\alpha)_{\text{LPP},l}$, bound within

pairs of 10 TO and 10 LPP modes, and the order remains to be discussed in detail. Briefly, we note that the lowest-frequency mode, $\omega(\alpha)_{\text{LPP }10}$, is bound between the zero-frequency modes TO-IX and TO-X (the Drude contributions). The highestfrequency mode, $\omega(\alpha)_{LPP,1}$, is bound between LPP-1 and LPP-2, and all approach infinity when $\omega_p \to \infty$. Also shown here are the experimental data obtained in this work. Included in Fig. 3 are the LPP modes with $\omega_{\rm p}$ (black solid lines). At $\omega_p = 0$ all LPP modes emerge from an LO mode, recognizing that the Drude contributions for $\omega_{\rm p} = 0$ originate from two LO modes with zero frequency. All LPP modes are further bound by a TO mode, except for the two highest frequency modes which approach infinity. It is an interesting thought to consider the frequency at infinity as the virtual TO modes for the Drude contributions, which appear in reality at zero frequency. We further observe again that LPP modes 5, 6, and 9 cross frequencies of TO modes IV, V, and VIII, respectively. In Fig. 3 it can now be seen clearly that the crossings appear with a polarization direction of the respective LPP mode, and the polarization direction of the respective LPP at the crossing is perpendicular to the polarization direction of the TO mode being crossed.

The free charge carrier density parameters obtained from our ellipsometry analysis and the nominal free electron density parameters, N_d-N_a , provided by the crystal growers are given in the Supplementary Material. We note very good to excellent agreement. Note that all electrical Hall measurements were performed on different pieces than those investigated here but cut from the same bulk crystals. Due to gradients in defect and dopant densities across the Czochralski grown crystals occasional deviations seen between our optical results and those reported from electrical investigations are therefore not unexpected.

See supplementary material for details of the samples investigated, the experimental procedures, and the numerical values of all parameters determined in this work.

This work was supported in part by the National Science Foundation under award DMR 1808715, by Air Force Office of Scientific Research under award FA9550-18-1-0360, by the Nebraska Materials Research Science and Engineering Center under award DMR 1420645, by the Swedish Energy Agency under award P45396-1, the Swedish Research Council VR award No. 2016-00889, the Swedish Foundation for Strategic Research Grant Nos. FL12-0181, RIF14-055, EM16-0024, and the Swedish Government Strategic Research Area in Materials Science on Functional Materials at Linköping University, Faculty Grant SFO Mat LiU No. 2009-00971. M. S. acknowledges the University of Nebraska Foundation and the J. A. Woollam Foundation for financial support. We acknowledge Klaus Irmscher for critically reading of the manuscript.

¹M. Higashiwaki, K. Sasaki, H. Murakami, Y. Kumagai, A. Koukitu, A. Kuramata, T. Masui, and S. Yamakoshi, Semicond. Sci. Technol. 31, 034001 (2016).

²M. Higashiwaki and G. H. Jessen, Appl. Phys. Lett. **112**, 060401 (2018).
³C. Janowitz, V. Scherer, M. Mohamed, A. Krapf, H. Dwelk, R. Manzke, Z. Galazka, R. Uecker, K. Irmscher, R. Fornari, M. Michling, D. Schmeißer, J. R. Weber, J. B. Varley, and C. G. V. de Walle, New J. Phys. **13**, 085014 (2011).

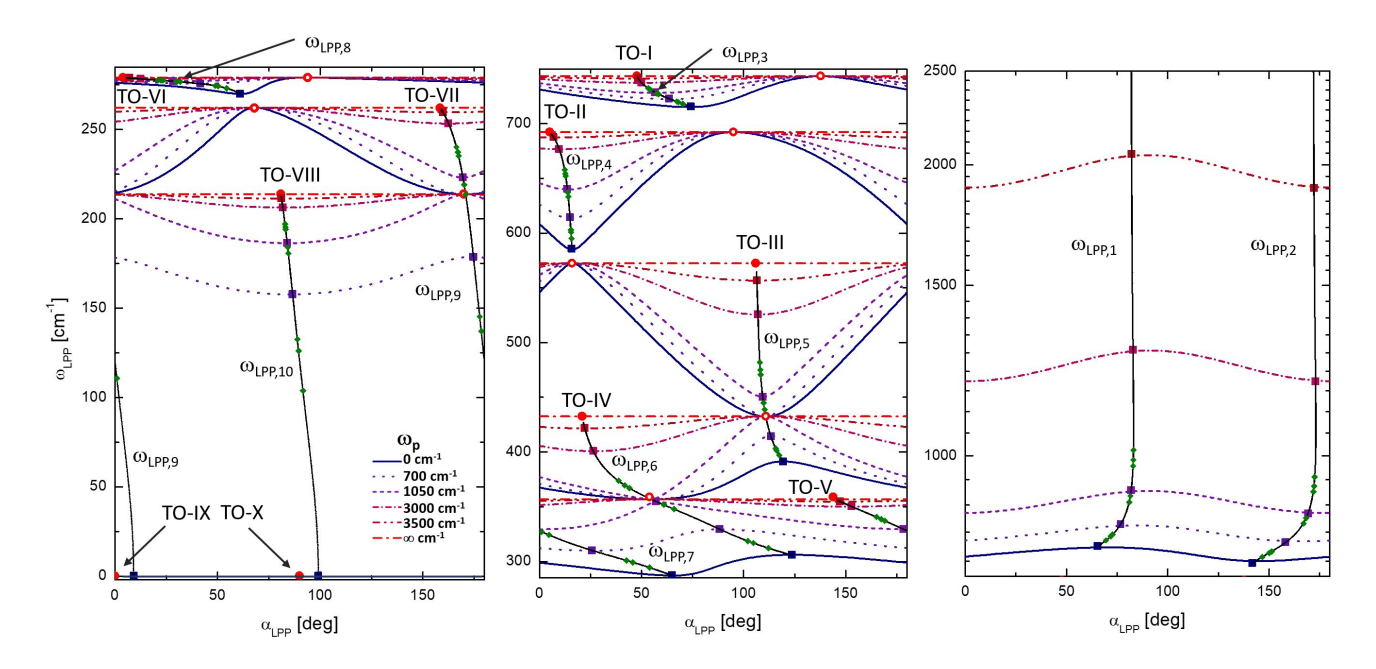


FIG. 3. Colored lines with different styles: B_u -symmetry directional limiting frequencies, $\omega(\alpha)_{\text{LPP},l}$, for β -Ga₂O₃ as a function of displacement direction, α , relative to axis a within the monoclinic plane, for selected plasma frequency parameters (see inset for labels). Black solid lines indicate the evolution of LPP modes as a continuous function of ω_p . Square symbols indicate B_u -symmetry LPP modes. Left panel: Modes $\omega(\alpha)_{\text{LPP},8}$ - $\omega(\alpha)_{\text{LPP},10}$, middle panel: modes $\omega(\alpha)_{\text{LPP},3}$ - $\omega(\alpha)_{\text{LPP},7}$, right panel: modes $\omega(\alpha)_{\text{LPP},1}$ and $\omega(\alpha)_{\text{LPP},2}$. Note the different y axis scales. Full red circles and numerals indicate B_u -symmetry TO modes. Open red circles indicate the TO frequencies at orientations perpendicular to the lattice TO mode polarization. Green diamonds indicate the experimental data observed in this work for LPP modes.

⁴C. Sturm, R. Schmidt-Grund, C. Kranert, J. Furthmüller, F. Bechstedt, and M. Grundmann, Phys. Rev. B **94**, 035148 (2016).

⁵C. Sturm, J. Furthmüller, F. Bechstedt, R. Schmidt-Grund, and M. Grundmann, APL Mater. 3, 106106 (2015).

⁶J. Furthmüller and F. Bechstedt, Phys. Rev. B **93**, 115204 (2016).

⁷A. Mock, R. Korlacki, C. Briley, V. Darakchieva, B. Monemar, Y. Kumagai, K. Goto, M. Higashiwaki, and M. Schubert, Phys. Rev. B **96**, 245205 (2017).

⁸Z. Galazka, Semicond. Sci. Technol. **33**, 113001 (2018).

⁹U. Betz, M. K. Olsson, J. Marthy, M. Escola, and F. Atamny, Surf. Coat. Technol. **200**, 5751 (2006).

¹⁰C. G. Granqvist, Handbook of Inorganic Electrochromic Materials (Elsevier, 1995).

¹¹D. Gogova, A. Iossifova, T. Ivanova, Z. Dimitrova, and K. Gesheva, J. Cryst. Growth **198/199**, 1230 (1999).

¹²F. Réti, M. Fleischer, H. Meixner, and J. Giber, Sens. Actuators, B Chem. 19, 573 (1994).

¹³J.-H. Yoo, S. Rafique, A. Lange, H. Zhao, and S. Elhadj, APL Materials 6, 036105 (2018).

¹⁴M. Schubert, Infrared Ellipsometry on Semiconductor Layer Structures: Phonons, Plasmons and Polaritons, Springer Tracts in Modern Physics, Vol. 209 (Springer, Berlin, 2004).

¹⁵B. B. Varga, Phys. Rev. **137**, A1896 (1965).

Kittel, Introduction To Solid State Physics (Wiley India Pvt. Ltd, 2009).
 M. Grundmann, The Physics of Semiconductors (Springer, Berlin Heidelberg, 2016).

¹⁸C. G. Olson and D. W. Lynch, Phys. Rev. **177**, 1231 (1969).

¹⁹N. K. S. Gaur, Physica B+C **82**, 262 (1976).

 R. J. Bell, T. J. McMahon, and D. G. Rathbun, J. Appl. Phys. 39, 48 (1968).
 M. Göppert, F. Gehbauer, M. Hetterich, J.Münzel, D.Queck, and C.Klingshirn, J. Luminesc. 72–74, 430 (1997).

²²P. Perlin, J. Camassel, W. Knap, T. Taliercio, J. C. Chervin, T. Suski, I. Grzegory, and S. Porowski, Appl. Phys. Lett. 67, 2524 (1995).

²³ A. Kasic, M. Schubert, Y. Saito, Y. Nanishi, and G. Wagner, Phys. Rev. B

65, 115206 (2002).

²⁴Y. Ishitani, M. Fujiwara, X. Wang, S.-B. Che, and A. Yoshikawa, Appl. Phys. Lett. **92**, 251901 (2008).

²⁵ M. Feneberg, C. Lidig, K. Lange, M. E. White, M. Y. Tsai, J. S. Speck, O. Bierwagen, and R. Goldhahn, phys. stat. sol. a 211, 82 (2014).

²⁶M. Schubert, R. Korlacki, S. Knight, T. Hofmann, S. Schöche, V. Darakchieva, E. Janzén, B. Monemar, D. Gogova, Q.-T. Thieu, R. Togashi, H. Murakami, Y. Kumagai, K. Goto, A. Kuramata, S. Yamakoshi, and M. Higashiwaki, Phys. Rev. B 93, 125209 (2016).

²⁷M. Schubert, A. Mock, R. Korlacki, and V. Darakchieva, Phys. Rev. B 99, 041201(R) (2019).

²⁸K. Ghosh and U. Singisetti, Appl. Phys. Lett. **109**, 072102 (2016).

²⁹K. Ghosh and U. Singisetti, J. Mat. Res. **32**, 4142 (2017).

³⁰K. Ghosh and U. Singisetti, J. Appl. Phys. **122**, 035702 (2017).

³¹A. Parisini, K. Ghosh, U. Singisetti, and R. Fornari, Sem. Sci. Tech. 33, 105008 (2018).

³²P. Yu and M. Cardona, *Fundamentals of Semiconductors* (Springer, Berlin, 1999).

³³M. Born and K. Huang, *Dynamical Theory of Crystal Lattices* (Clarendon, Oxford, 1954).

³⁴M. Schubert, Phys. Rev. Lett. **117**, 215502 (2016).

³⁵ A. Mock, R. Korlacki, S. Knight, and M. Schubert, Phys. Rev. B 95, 165202 (2017).

³⁶ A. Mock, R. Korlacki, S. Knight, and M. Schubert, Phys. Rev. B 97, 165203 (2018).

³⁷S. Knight, A. Mock, R. Korlacki, V. Darakchieva, B. Monemar, Y. Kumagai, K. Goto, M. Higashiwaki, and M. Schubert, Appl. Phys. Lett. 112, 012103 (2018).

³⁸We note that modes shown in Fig. 13 in Ref. 26 were accidentally calculated with the coordinate axes *x* and *y* exchanged. Figure 1c in this present work depicts the correct angular orientations.

³⁹G. Venkataraman, L. A. Feldkamp, and V. C. Sahni, *Dynamics of Perfect Crystals* (The MIT Press, Cambridge, Massachusetts, and London, England, 1975).